3D PRINTING

Three-dimensional nanofabrication via ultrafast laser patterning and kinetically regulated material assembly

Fei Han[1,2]*, Songyun Gu[1]*, Aleks Klimas[3], Ni Zhao[2,4], Yongxin Zhao[3]†, Shih-Chi Chen[1,2,5]†

A major challenge in nanotechnology is the fabrication of complex three-dimensional (3D) structures with desired materials. We present a strategy for fabricating arbitrary 3D nanostructures with a library of materials including metals, metal alloys, 2D materials, oxides, diamond, upconversion materials, semiconductors, polymers, biomaterials, molecular crystals, and inks. Specifically, hydrogels patterned by femtosecond light sheets are used as templates that allow for direct assembly of materials to form designed nanostructures. By fine-tuning the exposure strategy and features of the patterned gel, 2D and 3D structures of 20- to 200-nm resolution are realized. We fabricated nanodevices, including encrypted optical storage and microelectrodes, to demonstrate their designed functionality and precision. These results show that our method provides a systematic solution for nanofabrication across different classes of materials and opens up further possibilities for the design of sophisticated nanodevices.

In the field of nanotechnology, multimaterial three-dimendional (3D) fabrication at nanoscale has been a long sought-after goal (*1*, *2*). Most 3D nanofabrication techniques rely on lithographic methods to create complex structures with nanoscale resolution, in which photoinitiated chemical reactions such as photopolymerization (*3*–*5*) and photoreduction (*6*–*8*) are critical. Despite many previous attempts, material choices for nanofabrication are still largely limited to polymeric materials or metals. A fabrication solution for a wider class of materials without compromising existing structural complexity, nanoscale feature sizes, and material functions remains a critical challenge.

Fabrication of designed 3D nanostructures through direct assembly of materials has become an effective nanofabrication strategy. A prerequisite of the method is to selectively control the movement and subsequent integration of the material building blocks, such as nanoparticles (NPs) or macromolecules, with nanoscale precision. To this end, the driving force that governs the material assembly is critically important. Recent advances have demonstrated assembling charged metal particles with electrical fields (*9*–*11*), stacking blocks of nucleic acid with base pairings (*12*–*14*), or covalently linking dye molecules to a hydrogel, followed by attaching materials to the dyes (*15*). In principle, such bottom-up processes should be generally applicable in growing nanostructures of any material. Despite the straightforward strategy, none of the existing methods offer a generalizable solution. Particles from different materials always have distinctively different physical or chemical properties, and to systematically manipulate their assembly within a singular system is impossible due to the lack of suitable driving forces.

A hydrogel can capture a variety of materials through their different interactions, such as hydrogen bonds, charge effects, covalent bonds, or through their dense scaffolds. Thus, hydrogels can be used to form composites with different nanomaterials for 3D printing (*16*), or to support in situ photoreduction of metal NPs for nanopatterning (*17*). Moreover, by exposing a hydrogel with femtosecond (fs) laser, designed patterns can be labeled on the gel with two-photon reactions and additional photoreactive molecules (*18*–*20*). By engineering the molecular structures of these molecules in combination with the shrinking of gel substrates (implosion fabrication), certain functional materials can be bridged to the patterned gel through the coordination effect or hydrogen bonds with resolution beyond the optical diffraction limit (*15*).

We report a strategy to directly create arbitrary 3D patterns of various materials in hydrogel through the kinetic effects enabled by programmable fs light sheets (*21*, *22*). Previously, the optical system was used for two-photon lithography to generate 3D polymeric micro- and nanostructures. In this work, we found that its ultrahigh peak intensity ($> 1\ \mathrm{TW/cm^2}$) can directly modify the polymeric network of a polyacrylate-polyacrylamide hydrogel (*15*, *23*) in pure water (Fig. 1B), leading to reduced scaffold density and improved capability of forming hydrogen bonds at the exposed site. We exploited this phenomena to pattern the gel with designed 3D geometries and then selectively assembled material particles to the sites through regioselectivity induced by the size-dependent steric effect, or by the increasing density of hydrogen bonds. As this method uses kinetic factors to directly assemble materials (instead of tailored bridging molecules or conjugation reactions), our strategy can be extended to water-dispersible materials with suitable sizes (table S1) or hydrophilicity. To verify this point, we fabricated various 3D structures with a library of materials including metals, alloys, 2D materials, upconversion materials, diamond, molecular crystals, oxides, semiconductors, biomaterials, polymers, fluorescent species, and even inks from fountain pens. In addition, features of the patterned gels can be preadjusted before material deposition to achieve sub–diffraction limit resolution (20 to 35 nm). The assembled material particles were densely packed to form 3D structures with an exterior surface roughness of < 5 nm and a material filling ratio of ~60% by volume, which is suitable for nanodevice fabrication.

Schematics illustrating the fabrication steps are shown in Fig. 1, A to D, and fig. S1 (*24*). We first patterned an expanded hydrogel with our fs light sheet patterning system (*21*). A 100-fs laser beam from a 1-kHz regenerative amplifier is shaped and dispersed through a digital micromirror device (DMD), and then projected to the gel as a temporally focused light sheet for rapid patterning (Fig. 1E and fig. S2). The patterned gel was then incubated in the solution of the target material for 2 hours. This allowed for volumetric self-assembly of material particles onto the predefined patterns, generating 3D structures with submicrometer resolution (Fig. 1G).

Alternatively, as acrylic acid–based hydrogels shrink in acid, the patterned gel can be preshrunk in hydrochloric acid (4 mM) before material deposition, and then air-dried to create small features below the diffraction limit (Fig. 1C). Isotropic substrate shrinkage can be achieved by affixing the gel on a thin copper wire (fig. S3); the lateral and axial contraction ratios are measured to be 12.8 ± 0.4 and 12.7 ± 0.7 (mean ± SD, $n = 10$), respectively (fig. S4). After material deposition and dehydration, the small features can be characterized by scanning electron microscopy (SEM) (Fig. 1, H and I). Although the hydrogel scaffolds were kept for structural support in our demonstrations, cleavable cross-linkers (*25*), sintering (*26*), or chemical etching (*27*) may be used to remove the gel in some applications where a permanent scaffold is not desired.

Different from previous methods that pattern hydrogels through two-photon reactions with certain organic molecules (*15*, *18*–*20*), the

---

[1] Department of Mechanical and Automation Engineering, The Chinese University of Hong Kong, Shatin, Hong Kong. [2] Oxford-CityU Centre for Cerebro-Cardiovascular Health Engineering (COCHE), Shatin, N.T., Hong Kong. [3] Department of Biological Sciences, Carnegie Mellon University, Pittsburgh, Pennsylvania 15213-3815, United States. [4] Department of Electronic Engineering, The Chinese University of Hong Kong, Shatin, Hong Kong. [5] Centre for Perceptual and Interactive Intelligence (CPII), Shatin, N.T., Hong Kong.

*These authors contributed equally to this work.

†Corresponding author. Email: scchen@mae.cuhk.edu.hk (S.-C.C.); yongxinz@andrew.cmu.edu (Y.Z.)

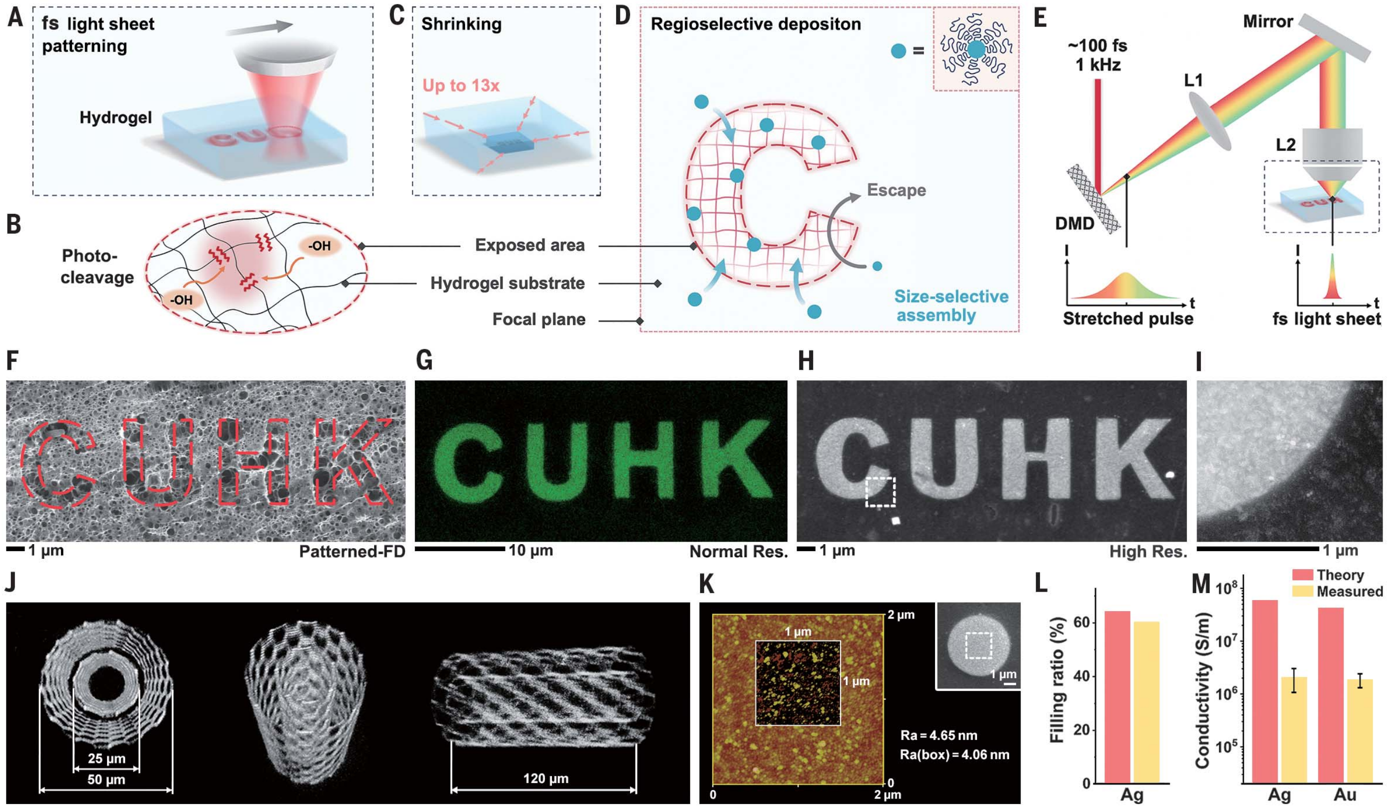

Fig. 1. Fabrication setup, process, and results. Schematics illustrating (**A**) the patterning process, in which complex patterns can be defined with a single exposure; (**B**) photocleavage of the polymer network of a hydrogel during patterning; (**C**) shrinkage of the patterned gel to reduce the feature size; and (**D**) regioselective deposition of materials in a shrunk gel through size selective assembly. (**E**) Configuration of the fs light sheet patterning system. L1: collimating lens; L2: objective lens. (**F**) SEM image of a fully shrunk and freeze-dried (FD) gel showing network structures on the "CUHK" pattern. (**G**) Fluorescent image of the "CUHK" pattern deposited with graphene QDs without preshrinking. SEM images of (**H**) the "CUHK" pattern deposited with Ag NPs (15 nm) after preshrinking the gel. (**I**) Zoomed in view of (G). (**J**) Top, tilted, and side views of a double-walled carbon nanotube structure assembled by fluorescein. (**K**) Atomic force microscopy measurements of a silver disk (shown in the inset). (**L**) Volume filling ratio of Au, TiO_2, and Fe_3O_4 in a 3×3×3 μm^3 cube; the theoretical value refers to random close packing (~64%). (**M**) Conductivity of the fabricated metal structures after laser sintering; error bars indicate mean ± SD ($n = 8$).

average light intensity (300 to 1000 W/cm^2) of the fs light sheets is high enough to directly modify the gel network in pure water for pattern definition. To explore how laser irradiance modified its microstructures, we characterized a patterned gel with SEM. The gel was shrunk and freeze-dried to remove the retention water. The results showed that the hydrogel substrate was partially etched at the patterned sites (Fig. 1F), leaving more porous network structures than the unexposed region. As its degree of porosity roughly increases with increasing laser doses (fig. S5), and the system contains no photosensitive species, it is possible that the gel scaffolds were partially removed through direct photodisruption (*28*) of its polymeric chains under the high-power laser.

X-ray photoelectron spectroscopy measurements indicated that the ratio of oxygen to carbon increased for ~49% after patterning (fig. S6), suggesting that the chemical components were modified. Interestingly, both Fourier-transform infrared (FTIR) spectroscopy and Raman spectroscopy indicated that the major chemical bonds of the gel remained unchanged (fig. S7). Only the FTIR spectrums showed a new peak at 1294 cm^{-1}, possibly corresponding to the stretching of C–O–H bonds. We further found that the laser for patterning is strong enough to directly excite the exposed water molecules (*29*, *30*), which can dissociate them into hydroxyls and free protons by 12% or more (*29*). As the photoexcited species should be highly reactive, we speculate that during the cleavage of hydrogel scaffolds, the simultaneously excited hydroxyls may connect to the partially disrupted polymer network (Fig. 1B), thereby contributing to the new peak in FTIR.

The addition of hydroxyls is expected to increase the formation of hydrogen bonds at the exposed sites. We exploited this effect to selectively attach suitable materials to construct 3D nanostructures. We designed a set of Chinese zodiac animals as test patterns to examine our method (fig. S10A). Six of the patterns were deposited with different hydrophilic materials to promote the formation of hydrogen bonds, including two dragons of CdSe quantum dots (QDs) (Fig. 2A), where the stripes show a feature size of 200 nm, a tiger of graphene QDs, a goat of fluorescent gold, a horse of fluorescent polystyrene spheres, a rooster of fluorescein, and a mouse of protein (Fig. 2, I-M). By tuning the laser dosage, the density of hydrogen bonds can be fine-tuned to achieve precise grayscale control (fig. S8). The fluorescent imaging results indicate that these photoluminescent materials retain their functions after deposition, which suggests that the chemical structures of the QDs or macromolecules were not modified.

By contrast, we used the porous network to kinetically regulate the assembly of materials in a preshrunk hydrogel. As the patterned sites have reduced densities of polymer networks, NPs of suitable sizes can be selectively trapped there to form defined patterns (Fig. 1D). For example, we patterned a gel with a laser dose

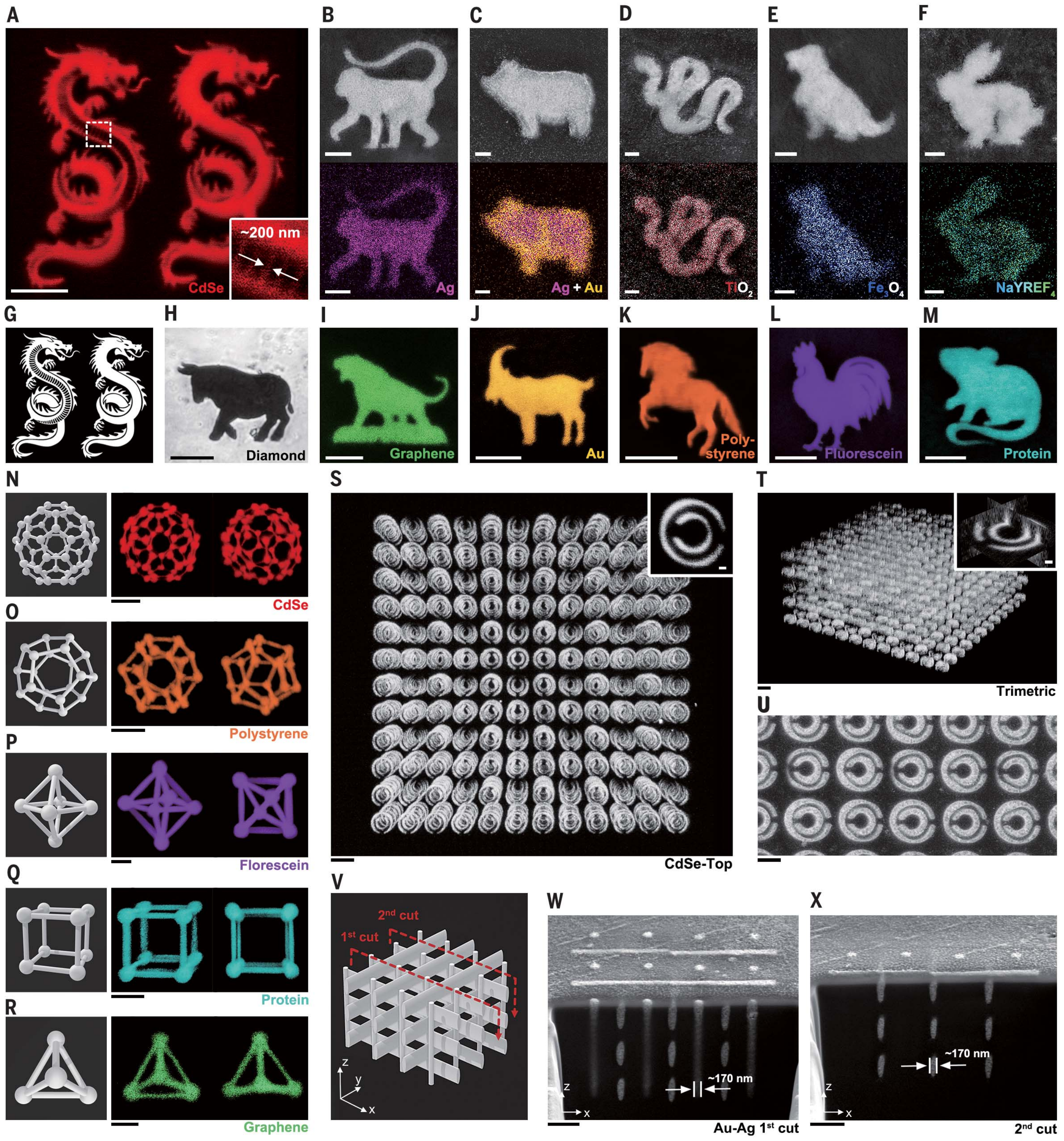

Fig. 2. Demonstration of material variety. (**A**) Fluorescent image of two dragons of CdSe QDs without shrinking; the inset shows a resolution of ~200 nm. (**B** to **F**) SEM (top) and EDX (bottom) images of a monkey of Ag, pig of Au-Ag alloy, snake of TiO_2, dog of Fe_3O_4, and rabbit of $NaYREF_4$, respectively. (**G**) Designed dragon patterns in (A). (**H**) Optical microscopy image of an ox of diamond. (**I** to **M**) Fluorescent images of a tiger of graphene QDs, a goat of fluorescent Au, a horse of polystyrene, a rooster of fluorescein, and a mouse of fluorescent protein, respectively. (**N** to **R**) 3D models and fluorescent images (maximum intensity projection) of the fabricated structures in shapes of a C_{60} molecule, regular dodecahedron, regular octahedron, cube, and regular tetrahedron of different materials, respectively. (**S**) Top view of a five-layer split ring resonator (SRR) structure; inset: SRR unit. (**T**) Trimetric view of the SRR structure in (S); inset: slice view of an SRR unit. (**U**) SEM image of the top layer of an SRR structure after shrinking and dehydration. (**V**) 3D model of a woodpile structure containing 16 vertical rods along the z axis. (**W** and **X**) SEM cross-sectional images of the fabricated woodpile at the two cut planes in (V), respectively. (Substrate tilt angle: 52°). Scale bars are 1 μm for (B to F, U, W, X, and the insets of S and T), and 10 μm for (A, H to M, and N to T).

of 600 W/cm^2 and 50 ms, into which we deposited gold NPs of different sizes. SEM images (fig. S9, A to F) showed that the 15- and 30-nm NPs were densely packed on the patterns to form designed geometries, whereas the 5-nm NPs failed to fill the patterns due to their much smaller size and limited steric hindrance. These results suggest that for a given laser dose, the deposition quality critically depends on the size of the NPs (see notes of fig. S9 for details). Additionally, as the porosity of the patterned network is determined by the laser dose, one may deposit smaller NPs with reduced doses (for example, 3 nm) (table S5). To precisely control the assembly toward ordered patterns, we varied the kinetic barrier of NP migration from the perspectives of entropy, restricting Brownian motion, and the repulsive surface charges. Specifically, the hydrogen bonds and steric effect were exploited to selectively reduce the barrier by providing adhesive forces to overcome electrostatic repulsion, or to suppress random aggregation elsewhere by trapping the NPs in the network, promoting selective assembly at the patterned sites. Notably, the steric effect can be further strengthened to improve the fabrication; encapsulating NPs with bulky ligands can increase selectivity during assembly (*31*, *32*) by introducing additional steric hindrance. For example, comparing with small-molecule ligands like citrate, functionalizing the gold NPs with polyvinylpyrrolidone (PVP) results in better structures with well-defined boundaries, smooth surfaces, and fewer background particles (fig. S9, E to G). PVP is a sizable ligand with long chains and multiple binding sites (Fig. 1D, inset); therefore, the interior NPs can be readily tethered to the porous network or each other (*33*), kinetically promoting their assembly and subsequent integration. The other kinetic factor, hydrogen bonding, still affects the process, and highly hydrophilic ligands such as hydroxyls should be avoided to prevent the retention of NPs on the substrate (fig. S9, F to I).

To demonstrate that steric control is generally applicable to materials of different chemical or physical properties, we deposited different NPs into the remaining six zodiac animals (see table S5 for detailed fabrication parameters), including a monkey of silver (Fig. 2B), a snake of TiO_2, a dog of Fe_3O_4, a rabbit of upconversion material [$NaYREF_4$ (RE: Yb, Er, Tm, Gd, Mn, Lu)], and an ox of diamond (Fig. 2, D to F and H, respectively). The method also allows for fabrication of alloy structures, such as gold-silver alloy (Fig. 2C) and TiO_2-Fe_3O_4 alloy (fig. S10F), by directly incubating the gel with a mixed solution of two NPs. The SEM images show that the structures do not have visible distortion at high shrinkage ratios, producing patterns of the designed shapes. The fabrication results were further confirmed by energy-dispersive x-ray (EDX) mappings (fig. S10 and S11). Notably, such kinetic control is not limited to the aforementioned species. Fabrication of other materials, such as sulfur, platinum, zinc sulfide, and even fountain pen inks, can generally be achieved by choosing appropriate combinations of particle sizes and laser doses (fig. S12).

Next, we demonstrate our capability in fabricating complex 3D structures of different materials and feature sizes. First, a series of polyhedrons were sequentially patterned and deposited with different materials without preshrinking the gel, including a C_{60} model of CdSe, a regular dodecahedron of fluorescent polystyrene, a regular octahedron of fluorescein, a cube of protein, and a regular tetrahedron of graphene (Fig. 2, N to R). As the materials are assembled volumetrically, when combined with the fs light sheet system, the method allows rapid fabrication of large-area 3D structures, such as a five-layer, spatially separated split ring resonator array with 720 individual units in a volume of $1.44 \times 10^7\ \mu m^3$ (Fig. 2, S to U). Notably, the patterning process was completed in only 0.18 seconds with our system [patterning rate of ~300 mm^3/hour or ~1.6×10^8 voxel/sec (*21*)], which usually needs minutes to hours in a conventional point-scanning system (*3*, *15*). Aside from the high patterning rate, our method also realizes self-alignment for multilayer printing. This enables the creation of arbitrary, unconnected 3D structures, which could not be readily achieved previously. Examples of millimeter-scale complex 3D structures are presented in fig. S13.

To verify that the morphology of the fabricated structures can be retained in all three dimensions in preshrunk hydrogels, we fabricated a modified woodpile structure of gold-silver alloy, which contains 16 vertical rods along the z axis (Fig. 2V). Our SEM images showed that the structure has a well-defined top surface without visible distortion (fig. S14E). We applied a focused ion beam (FIB) to section and evaluate the interior of the structure, which confirmed that the materials were densely packed inside the woodpile structure with good geometric accuracy (Fig. 2, W and X, and fig. S13, B to D). More results of woodpile structures of different scales are presented in fig. S14 and S15.

To investigate the fabrication resolution, we designed a series of 2D and 3D nanostructures. First, we fabricated arrays of four nanowires with projected widths of 7, 5, 3, and 2 pixels (px) on the DMD, respectively (Fig. 3C). The DMD pixel has a pitch of 7.56 μm, which maps to 94.5 nm in the build plane. Because the diffraction limit of the patterning system is 340 nm (calculated with the Rayleigh criterion), and the hydrogel has a shrinkage ratio of ~13, the corresponding minimal feature size after preshrinking is estimated to be ~25 nm. To match the scale, 5-nm silver NPs were used in the fabrication in combination with lower laser doses (500 W/cm^2 and 5 ms) (Fig. 3E). Figures 3, A and B, presents a representative nanowire array. We measured the widths of the wires (A to C) from both the SEM images and the gray level profiles (Fig. 3F), in which their full widths at half maximum (FWHMs) were 19.0, 23.5, and 39.0 nm, respectively. The top wire in Fig. 3A, which was defined by only 2 px, shows uneven width. We attribute this potentially to insufficient laser intensity: As the width of the projected wires reduces, their FWHM at the focal plane converges to the diffraction limit, and the corresponding intensity decreases (Fig. 3, D and E). Thus, the simulated intensity of the thinnest wire is approximately one-half of that of wire A, and only approximately one-quarter of that of wire C, which is too weak for uniform pattern creation. A survey that we performed of 10 groups of such arrays shows the widths of the wires (A to C) are 21.1 ± 5.0, 29.2 ± 3.0, and 37.7 ± 2.8 nm (mean ± SD), respectively, indicating that the fabrication is highly reproducible even at its limit.

We designed and fabricated a nonconnected 3D “NANO” structure consisting of arrays of parallel nanowires (Fig. 3H) to examine whether the same small feature size can be achieved in a complex 3D structure. Each nanowire had a projected width of 6 px on the DMD, and thus we estimated the final feature size to be ~35 nm. After fabrication with 5-nm silver NPs, we applied the FIB to section and evaluate the “NANO” structure (Fig. 3, I to K), where we found that the nanowires were accurately positioned without distortion. Our FWHM measurements of the linewidth produced an average lateral and axial resolution of 36.0 ± 5.1 and 148.4 ± 19.2 nm (mean ± SD, $n = 20$), respectively (Fig. 3L). This is consistent with the fabrication results of a 16-layer woodpile structure [with the same designed linewidth as the “NANO” structure (fig. S15)] and agrees with the simulation (fig. S2C), in which one may observe that the voxel aspect ratio increases with increasing projected linewidths.

The density of the deposited material is an important metric in evaluating the fabricated structures. We first performed AFM measurements on the exterior surface of the dehydrated material-deposited gels. The results showed high levels of smoothness, such that the mean surface roughness of the gold and silver structures only measured 4.69 and 4.06 nm, respectively (Fig. 1K and fig. S18), which suggests high material density. This smoothness is among the best reported results across all 3D printing and nanofabrication methods (See discussions in fig. S18). To characterize the material density in a 3D structure, we next fabricated a 3 μm^3 cube with 15-nm silver NPs, to which FIB was applied to section and examine the interior (fig. S16, B to D). The results confirm that the silver NPs

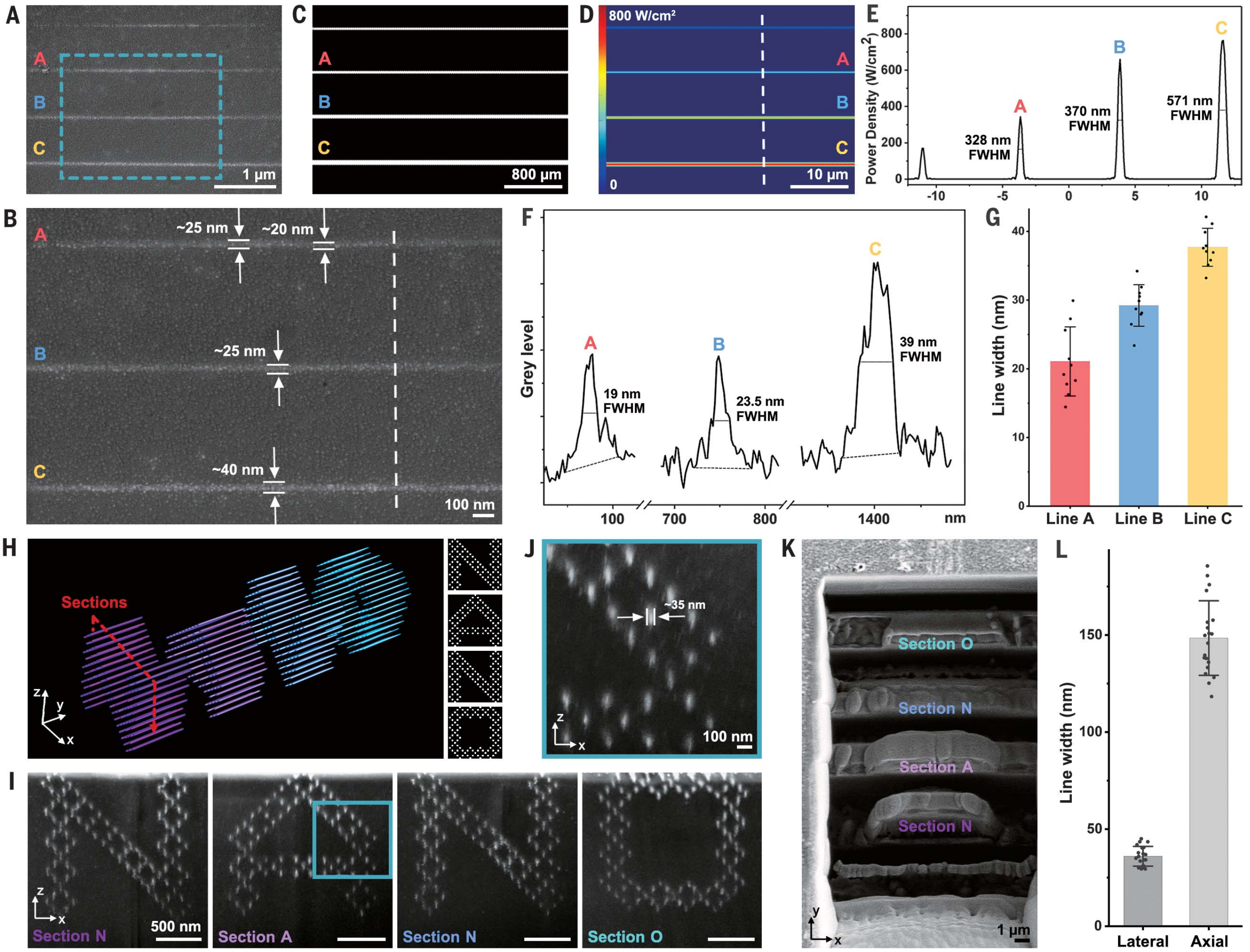

Fig. 3. Nanostructures demonstrating minimum feature sizes. SEM images of (**A**) an array of nanowires fabricated with 5-nm silver NPs, and (**B**) a zoomed-in view of (A). (**C**) Pattern displayed on the DMD. (**D**) Simulated intensity distribution at the build plane. (**E**) Cross-sectional profiles showing the intensity distribution in (D). (**F**) Grey level profiles of nanowires A to C across the dashed line in (B), which provide more accurate measurements. (**G**) Measurements of the linewidths in ten nanowire arrays. (**H**) 3D model of a nonconnected "NANO" structure comprised of arrays of parallel nanowires; and its four cross-sectional patterns (on the *x-z* plane). (**I**) SEM cross-sectional images of the "NANO" structure cut by FIB; and (**J**) a zoomed-in view of the letter "A" in (I). (**K**) SEM images showing the trenches of the gel sample opened by the FIB cut, in which the positions of each letter are labeled. All cross-sectional images were taken at a substrate tilt angle of 52°. (**L**) Survey of 20 different linewidths in 3D structures measured from (I) and fig. S15; error bars indicate mean ± SD.

are highly uniform and densely packed inside the cube. EDX mapping of a 1 μm^2 area of the section showed that the volume fraction of silver is 60.2% (fig. S16E), which reached ~94% of the theoretical density, assuming random close packing. Further experiments show that our method can also achieve high volume-filling ratio for non-metal materials, such as 61.3% and 58.3% for TiO_2 (5 nm) and Fe_3O_4 (10 nm), respectively (Fig. 1L and fig. S17).

Because the target materials are only applied in the last fabrication step, their original properties and functions can be preserved. We investigated the properties of fabricated metal structures, which are widely used in nanoscience, and demonstrated their potential applications. We tested the conductivity of different metals in preshrunk hydrogels, such as silver, gold, and gold-silver alloy (atomic ratio of 1:1). After material dehydration, an 80-MHz fs laser was applied to sinter the assembled NPs and to remove any ligands that may influence conductivity (fig. S19). The sintered structures were highly conductive, possibly owing to the high material-filling fraction. The silver, gold, and gold-silver alloy achieved conductivity of 2.06×10^6, 1.86×10^6, and 2.16×10^4 S/m, respectively, which allowed for the fabrication of conductive microelectrodes (fig. S20). The high conductivity was also evidenced by the highly linear current-voltage (*I-V*) curves [coefficient of determination (R^2) > 0.999]. Such high conductivity levels are ideal for applications in sensors, catalysis, and microelectronics.

Because the hydrogels are optically transparent, our method can directly fabricate various optical microdevices, such as diffractive optical elements (DOEs). We designed a 200 by 200 px binary hologram (fig. S21A) that encodes a pair of symmetric smileys (Fig. 4B). The hologram was first projected to the hydrogel for pattern definition. The gel was then shrunk, followed by the deposition of silver (15 nm). After dehydration, the device was completed and had a pixel size of 500 nm (Fig. 4A and fig. S21, B to D). The hologram is binarized through the different optical densities; the silver-deposited sites represent "0" and the empty sites represent

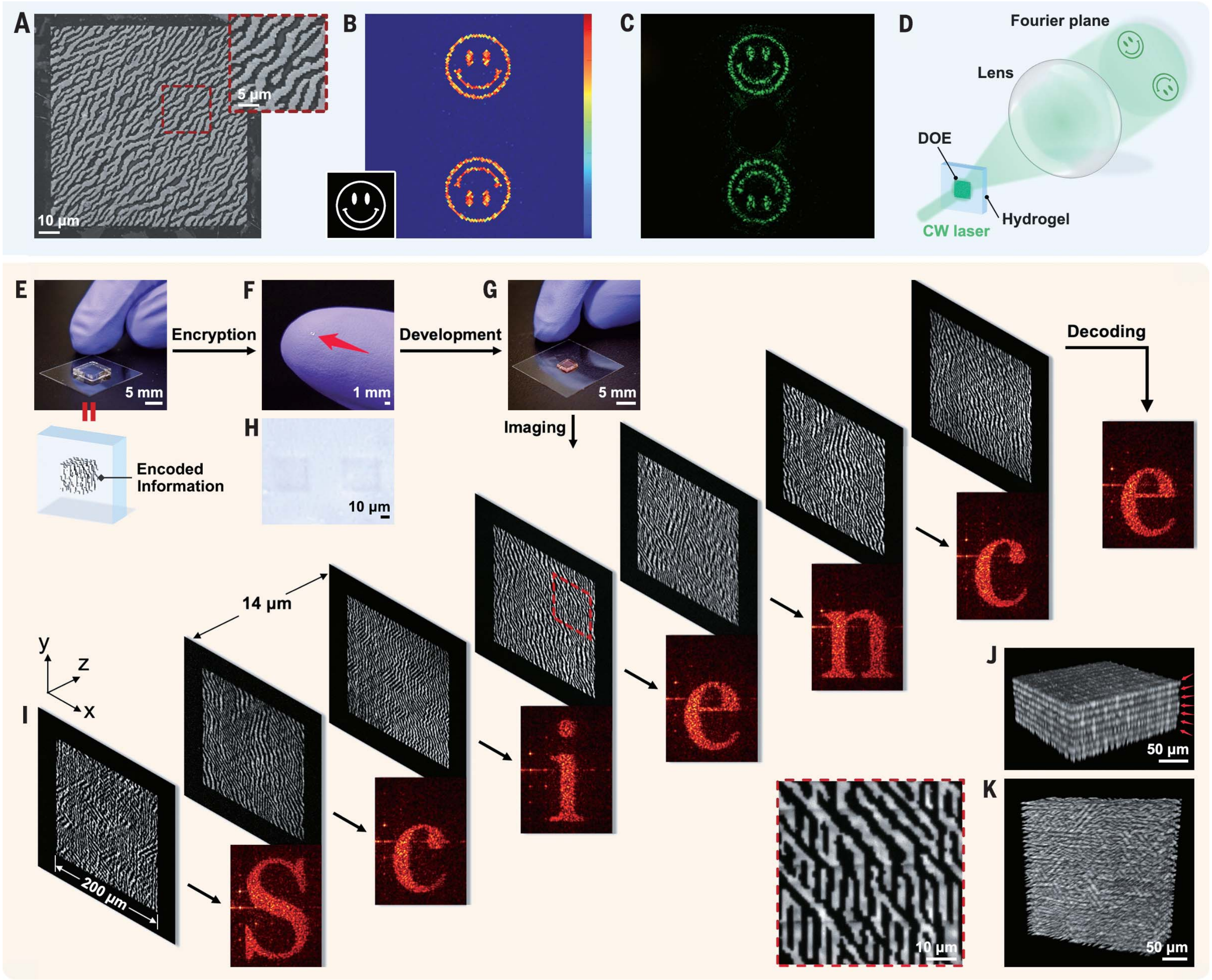

Fig. 4. Fabrication of DOE and applications in 3D optical storage and encryption. (**A**) SEM image and a zoomed-in view of a fabricated DOE. (**B**) Simulated intensity distribution at the Fourier plane of the DOE; inset: the encoded smiley. (**C**) Image recorded from the fabricated DOE in (A). The 0th order is spatially blocked to avoid camera damage. (**D**) Schematic of the optical setup to record the encoded image. (**E** to **G**) Demonstration of optical storage and encryption: (E) an expanded hydrogel patterned with designed information; (F) the gel in (E) after full shrinkage and dehydration to realize physical encryption; (G) the re-expanded gel deposited with CdSe and developed to decrypt the stored patterns. (**H**) Optical image showing two encrypted seven-layer hologram patterns in (F). (**I**) Fluorescent images of the decrypted holograms, in which "Science" is decoded; and (**J** and **K**) 3D views of the decrypted holograms.

"1" with a much higher transmission ratio. We collimated a 532 nm continuous wave laser to fully fill the aperture of the hologram, and recorded the reconstructed patterns on the observation screen (Fig. 4C). The reconstructed patterns show that the spatial frequency information of the device is well preserved during the large-area fabrication.

By exploiting the nanometer-level feature size and high laser patterning rate, we demonstrate an optical storage and encryption method by physically shrinking the optically written information in a 3D nanostructure. As a proof-of-concept demonstration, we designed and fabricated a seven-layer 3D structure that encodes "Science," where each layer contains a 200 by 200 px hologram that is encoded with a letter (pixel size 2000 nm) (fig. S23). The designed holograms were patterned in a fully expanded gel by means of the fs light sheet (Fig. 4E). After full shrinkage, each pixel of the structure was reduced to ~150 nm with a storage density of 20 terabits (Tb)/cm^3. Because the feature size was then below the diffraction limit and 3D in nature, information stored in the structure was effectively encrypted. When structures with reduced thickness are patterned, they are completely invisible (fig. S24C). Only a translucent rectangle without structural details could be observed under an optical microscope (Fig. 4H). Additionally, the shrunk and dehydrated hydrogels are chemically stable and can be stored over long periods of time.

To decrypt the structure, the device was re-expanded in a solution of NaOH (0.5 mM aq.) and deposited with CdSe QDs (or other fluorescent materials) to read out the stored holograms by confocal microscopy, which were subsequently decoded into "Science" (Fig. 4I). From these results, we confirmed that the stored holograms can be retrieved with high fidelity (Fig. 4, I to K, and fig. S23). Considering the high pattern rate of the fs light sheet, this approach has enabled an optical writing speed of up to 84 megabits (Mbit)/s and a theoretical storage density of ~5 petabits (Pbit)/cm^3 (by setting the pixel size to ~40 nm). The fs patterning system can be modified into a temporal focusing microscope (*34*) to achieve an optical reading speed of ~84 Mbit/s, which may create opportunities in the field of digital data storage. For example, in fig. S25, we demonstrated a storage density of 1.14 Pbit/cm^3, reaching the same order of magnitude of the theoretical limit.

In traditional nanoscience, direct assembly of materials into complex 3D structures requires complicated chemistry and/or a tailored printing setup. Our work demonstrates the delicate use of kinetic control in manipulating the assembly of a wide range of materials. In principle, the method can be readily extended to other water-soluble or -dispersible materials without further chemistry design. With advanced nanosynthesis methods (*35*), such as creating core-shell or composite structures, our method may work for materials that are unstable in water, such as perovskite. Its application scope may be further expanded by applying the strategy to other high-throughput optical platforms (*36*, *37*) or polarization optimizations (*38*). With the demonstrated throughput, resolution, and material generality, our new fabrication platform presents a disruptive solution in creating new functional and biocompatible microdevices, optical metamaterials, and flexible electronics that may impact the fields of photonics, nanotechnology, and biotechnology.

REFERENCES AND NOTES

1. H. Zhao *et al*., *Nano Today* **30**, 100825 (2020).
2. D. A. Walker, J. L. Hedrick, C. A. Mirkin, *Science* **366**, 360–364 (2019).
3. E. Skliutas *et al*., *Nanophotonics* **10**, 1211–1242 (2021).
4. J. F. Xing, M. L. Zheng, X. M. Duan, *Chem. Soc. Rev.* **44**, 5031–5039 (2015).
5. Y. L. Zhang, Q. D. Chen, H. Xia, H. B. Sun, *Nano Today* **5**, 435–448 (2010).
6. Y. Chen *et al*., *Nat. Commun.* **11**, 5334 (2020).
7. C. Barner-Kowollik *et al*., *Angew. Chem. Int. Ed.* **56**, 15828–15845 (2017).
8. J. Li, E. H. Hill, L. Lin, Y. Zheng, *ACS Nano* **13**, 3783–3795 (2019).
9. W. Jung *et al*., *Nature* **592**, 54–59 (2021).
10. M. S. Saleh, C. Hu, R. Panat, *Sci. Adv.* **3**, e1601986 (2017).
11. H. Lee *et al*., *Nano Lett.* **11**, 119–124 (2011).
12. L. L. Ong *et al*., *Nature* **552**, 72–77 (2017).
13. D. Han *et al*., *Science* **332**, 342–346 (2011).
14. S. Dey *et al*., *Nat. Rev. Methods Primers* **1**, 1–24 (2021).
15. D. Oran *et al*., *Science* **362**, 1281–1285 (2018).
16. S.SoleymaniEilBakhtiari *et al*., *Adv. Eng. Mater.* **23**, 2100477 (2021).
17. S. Kang, K. Vora, E. Mazur, *Nanotechnology* **26**, 121001 (2015).
18. C. A. DeForest, K. S. Anseth, *Angew. Chem. Int. Ed.* **124**, 1852–1855 (2012).
19. M. A. Skylar-Scott, M.-C. Liu, Y. Wu, A. Dixit, M. F. Yanik, *Adv. Healthc. Mater.* **5**, 1233–1243 (2016).
20. C. A. DeForest, K. S. Anseth, *Nat. Chem.* **3**, 925–931 (2011).
21. S. K. Saha *et al*., *Science* **366**, 105–109 (2019).
22. D. Kim, P. T. C. So, *Opt. Lett.* **35**, 1602–1604 (2010).
23. F. Chen, P. W. Tillberg, E. S. Boyden, *Science* **347**, 543–548 (2015).
24. Materials and methods are available as supplementary materials.
25. J. B. Chang *et al*., *Nat. Methods* **14**, 593–599 (2017).
26. L. R. Meza, S. Das, J. R. Greer, *Science* **345**, 1322–1326 (2014).
27. X. Zheng *et al*., *Nat. Mater.* **15**, 1100–1106 (2016).
28. S. Pradhan, K. A. Keller, J. L. Sperduto, J. H. Slater, *Adv. Healthc. Mater.* **6**, 1700681 (2017).
29. J. Xu, D. Chen, S. Meng, *J. Am. Chem. Soc.* **143**, 10382–10388 (2021).
30. M. F. Lin *et al*., *Science* **374**, 92–95 (2021).
31. Y. Wang, J. He, C. Liu, W. H. Chong, H. Chen, *Angew. Chem. Int. Ed.* **54**, 2022–2051 (2015).
32. F. Han *et al*., *J. Am. Chem. Soc.* **142**, 15396–15402 (2020).
33. H. Sun *et al*., *J. Am. Chem. Soc.* **135**, 9099–9110 (2013).
34. J. Jiang *et al*., *Opt. Express* **23**, 24362–24368 (2015).
35. H. Wang, L. Chen, Y. Feng, H. Chen, *Acc. Chem. Res.* **46**, 1636–1646 (2013).
36. M. Ren *et al*., *Opt. Express* **29**, 44250–44263 (2021).
37. L. Jonušauskas *et al*., *Opt. Express* **27**, 15205–15221 (2019).
38. S. Rekštytė *et al*., *Adv. Opt. Mater.* **4**, 1209–1214 (2016).

ACKNOWLEDGMENTS

We thank Dongmeng Su from the Nanyang Technological University for providing the Au NPs for initial experiments; X. Han for obtaining Raman spectrums; S. Liu for accessing the confocal microscope; H. Chen and Y. Zhu for the helpful discussions; X. Xu for information on preparing the hydrogels; and J. Yang for accessing the sourcemeter for conductivity measurements. **Fundings:** We acknowledge funding support from the HKSAR Research Grants Council, General Research Fund 14203020; Innovation and Technology Commission, Innovation Technology Fund ITS/178/20FP; Carnegie Mellon University faculty startup fund; and InnoHK Centre projects funded by the Innovation and Technology Commission A-CUHK-16-5-14 and COCHE-1.5. **Author contributions:** S.-C.C., Y.Z., and F.H. conceived the study. S.G. set up the fs light sheet patterning system and patterned the hydrogels. Y.Z. and A.K. prepared the hydrogels for the initial studies. F.H. and S.G. performed material deposition, characterization, and other experiments together. F.H. investigated the mechanism of material assembly. Y.Z., N.Z., A.K., S.G., and S.-C.C discussed and improve the mechanism. F.H. and S.G. optimized fabrication protocols. F.H. and S.G. prepared the manuscript with revisions from S.-C.C., N.Z., and Y.Z. **Competing interests:** A US patent application related to this work has been filed with S.-C.C., S.G., F.H., Y.Z., and A.K. as coinventors. All authors declare that they have no other competing interests. **Data and materials availability:** All data are available in the manuscript or the supplementary materials. **License information:**

SUPPLEMENTARY MATERIALS

science.org/doi/10.1126/science.abm8420
Materials and Methods
Figures S1 to S25
Tables S1 to S5
Movie S1
References (*39*–*42*)

Submitted 15 October 2021; resubmitted 7 June 2022
Accepted 21 November 2022
10.1126/science.abm8420

Three-dimensional nanofabrication via ultrafast laser patterning and kinetically regulated material assembly

Fei Han, Songyun Gu, Aleks Klimas, Ni Zhao, Yongxin Zhao, and Shih-Chi Chen

Science, **378** (6626), .
DOI: 10.1126/science.abm8420

Making many tiny things

Fabricating high-resolution and complex objects with additive manufacturing across a wide range of materials is challenging. Han *et al*. synthesized very finely detailed objects from a wide range of materials using femtosecond light sheets and nanoparticle-laden hydrogels. The strategy works for ceramics, polymers, metals, semiconductors, and other materials while still maintaining fine feature sizes. This technique could enable nanofabrication across different classes of materials. —BG

Science (ISSN) is published by the American Association for the Advancement of Science. 1200 New York Avenue NW, Washington, DC 20005. The title *Science* is a registered trademark of AAAS.